ISSN: 2977-0041

Research Article

Journal of Material Sciences and Engineering Technology

Nanofiltration Membranes Performance using Ion Transfer, Fouling Models and Techno-Economic Study

Noureddine Zouhri[1*], Mustapha Tahaikt[1], Abdelah Lachheb[1], Mahacine Elamrani[1] and Mohamed Taky[1,2*]

[1]*Laboratory of Advanced Materials & Processes Engineering, Department of Chemistry, Faculty of Sciences, Ibn Tofail University, P. O. Box 1246, Kenitra 14000 Morocco*

[2]*International Water Research Institute, Mohammed VI Polytechnic University, Lot 660, Hay Moulay Rachid Ben Guerir, 43150- Morocco*

[*]Corresponding author

Noureddine Zouhri, Mohamed Taky, Laboratory of Advanced Materials & Processes Engineering, Department of Chemistry, Faculty of Sciences, Ibn Tofail University, P. O. Box 1246, Kenitra 14000 Morocco.

Mohamed Taky, International Water Research Institute, Mohammed VI Polytechnic University, Lot 660, Hay Moulay Rachid Ben Guerir, 43150- Morocco.

Received: August 04, 2025; **Accepted:** August 29, 2025; **Published:** September 10, 2025

ABSTRACT

The water of M'rirt city (Moroccan town) which is coming from Oum Errabia sources has a conductivity of 2140 µS/cm which exceeds the World Health Organization (WHO) guidelines. This value of conductivity is attributed to the Na+ and Cl- concentrations. In this paper, the removal of Na^+, Cl^- and Ca^{2+} ions by Nanofiltration (NF) was studied. Three commercial NF membranes were tested. Applied pressure and recovery rate influence has been studied. Spiegler-Kedem (SK) model was used to estimate the two parameters of reflection coefficient σ and solute permeability P_s for the three ions and in two conversion rates of 30% and 40%. Steric Hindrance Pore (SHP) model was used to determine the effective pore size (r_p) and membrane thickness to porosity ($\Delta x/A_k$) parameters for the three ions and in two conversion rates of 30% and 40%. Hermia model applied in this study showed that fouling is of the cake type for the three membranes. This study showed a good agreement between resuts and experimental data for NF90*4040 membrane applying the combined cake formation-complete blocking pore model and which is confirmed by ANOVA statistical analysis. The produced cubic meter operating cost calculated for NF90*4040 membrane is 0.131 €/m^3 for a produced water with a sodium concentration of 150 mg/L.

Keywords: Spiegler-Kedem Model, Hermia Model, Steric Hindrance Pore Model, Anova Statistiques, Cost Evaluation

Introduction

Several regions in Morocco have salinity levels that exceed standards. The Lambert X (484000) and Y (285000) coordinates indicate that the town of M'rirt (Morocco), where our study is conducted, is located at 30 km northeast of the town of Khénifra [1]. Due to the existence of saline rocks, the water in this region is contaminated and is often brackish exceeding the standards. Sources of Oum Errabia River supplies city of M'rirt by water with an average conductivity of 2140 µS.cm^{-1}. The water in this city has a Na^+ and Cl^- content that exceeds the World Health Organization (WHO) standards.

Illness related with sodium insufficiency in humans are very infrequent. Nevertheless, long-term effects and acute health problems can be induced by excessive sodium [2]. In one reported case After receiving a dose of approximately 9200 mg Na/kg in the form of NaCl which iduced vomiting of 2-year-old boy who died 9 days later [3]. Despite medical intervention, death was occurred. The hospitalization of the child within 2 hours of saline administration was materialized. When the child was in a coma, his temperature was in high level, his breathing was fast and his heart rate leisurely and he was cyanotic and suffering from seizures [4-6]. Many researchers have tested, in children, the relationship between blood pressure and sodium intake from water. Majority of these studies did not find a relationship, in children, between high level of blood pressure and concentration of sodium in drinking water (concentration varying from 5 to 583 mg/L) and while a limited studies indicate

Citation: Noureddine Zouhri, Mustapha Tahaikt, Abdelah Lachheb, Mahacine Elamrani, Mohamed Taky. Nanofiltration Membranes Performance using Ion Transfer, Fouling Models and Techno-Economic Study. J Mat Sci Eng Technol. 2025. 3(3): 1-15. DOI: doi.org/10.61440/JMSET.2025.v3.69

an increase in blood pressure with high sodium intake [7-15]. People with kidney failure are easily affected with high sodium intake than people with healthy kidneys.

Chloride ion occurs naturally in the environment. The detection of high chloride concentrations in surface waters does not necessarily indicate the existence of an anthropogenic source. Natural sources of chlorides in aquatic systems include natural saline lakes and groundwater discharges from saline aquifers. In Canada, numerous evaporitic deposits of marine origin of natural salts are known [16]. In terms of water resources: Chlorides come first from precipitation where they are present thanks to evaporation in the oceans and certain industrial discharges. They reconcentrate by evapotranspiration in the soil before infiltrating. In certain sectors, chloride inputs are associated with salt formations and in coastal areas the intrusion of marine waters can contribute to increasing the content. Anthropogenic sources include fertilizers (KCl), certain industrial activities and landfill leachates [17]. The dissolution of minerals from sediments is the main cause of chlorides appear in natural waters [18]. Most natural waters contain chlorides in the form of calcium, magnesium and sodium salts [19].

The World Health Organization standards fixed maximum acceptable concentrations of sodium and chloride in drinking water at 200 mg/L and 250 mg/L respectively [20]. Ibn Tofail University (Morocco) in collaboration with National Office of Electricity and Potable water (ONEE) planned to reach WHO standards for drinking water in town of M'rirt by reducing the content of sodium and chloride ions and consequently reducing the salinity in drinking water of M'rirt city (Morocco) using membranes processes.

These processes present m any advantages in drinking water production. They allow production of water with consistent quality, and the use of chemical reagents because a wide range of pollutants are removal in single-step, and therefore by-products of treatment. Also, the quality of water produced by theses processes is better than that obtained by conventional processes. This quality remains stable. Large scale applications of these processes are now available [21]. High-pressure membrane process such as nanofiltration (NF) operates in high pressures ranging from 75 to 250 psi.

Molecular weight cut-off (MWCO) of NF membranes is typically ranges between 150 and 800 Da. NF process is actually used for the water treatment and progressively substituting the areas kept in reserve to RO like brackish water treatment. NF process is characterized by two mechanisms of mass transfer: the solubilization-diffusion and the convection [22]. The mechanism of retention of solutes in NF process is complex and until now is still not completely known. Many studies have been achieved, including modeling of NF process, to investigate mechanisms of transfer and retention of solutes. Many models were established for the description and prediction of retention and the flux of different charged and uncharged solutes using NF membranes. Mathematic models can be applied to determine effective thickness to porosity ratio, membrane pore size and membrane properties [23].

To predict and optimize NF membranes performance for ion rejection, mathematical models were applied. Nevertheless, solutions with two or three types of ions and dilute solutions have been examined until today by majority of modeling investigations [24].

Spiegler-Kedem (SK) mass transfer model presents, for solvent properties and for a given membrane, a relationship beween the flux and the solute concentration difference. In this model, and for individual ions in NF process, the experimental data of flux versus solutes retention is used to validate a model. In the Steric Hindrance Pore (SHP) model, the structural parameters of a membrane are associated to the SK model estimated parameters [24].

Nevertheless, in the applications of membrane technology, the main barrier is fouling which is unavoidable phenomenon. The performance of membranes systems can be affected by membrane fouling. The main categories of fouling occured in water purification technologies involve precipitation of inorganic salts, accumulation of suspended particulate matter and formation of a biofilm [25].

Membrane fouling corresponds to a decline in membrane permeability as a consequence of the flux resistance due to concentration polarization phenomenon, pore blocking and cake formation. Fouling mechanism has been demonstrated that is depending especially on the interactions that occur either between the particles or between the particles and the membrane. Also, the membrane fouling can cause a membrane irreversible blockage and a depreciation in the lifetime of the membrane. Based on the analysis, we find many approaches for modeling membrane effectiveness among them the approache of Hermia model (pore-blocking mechanisms in the membrane).

In filtration under constant pressure, the Hermia model permits determining the membrane fouling mechanism [26].

The flux reduction in membranes fouling can be caused by more than one individual fouling mechanisms. Thus, the combination of the membranes fouling mechanisms and their simultaneous effects on flux reduction had considerable attention. Ho and Zydney developed mathematical model for flux reduction during the purification of bovine serum albumin solution. In this study, Ho and Zydney found that the initial fouling mechanism was by complete blocking and in a result by cake formation mechanism [27].

In their work, Ho and Zydney used a method to develop combined models of fouling with two fitted parameters, among them the cake - complete blocking model which were assumed to be arised simultaneously [28].

Mansour Kazemimoghadam and Zahra Amiri-Rigi used the combined model to Ultrafiltration of Skim Milk. They studied the transmembrane pressure and temperature effects on flux reduction. The results of study showed that the combined model and the experimental data were in excellent agreement [29]. Also, cake filtration model can show good data fits and may be applied to solutions with solutes susceptible to accumulate as a cake layer on the membrane.

The purpose of the present paper is to follow and compare the performances of three commercial NF membranes in the removal of Na^+, Cl^- and Ca^{2+} concentration in continuous mode. In the M'rirt city drinking water treatment plant, NF/RO experimental pilot was installed downstream from the conventional treatment system. The range of pressure applied varies from 6-40 bar in our experiments. The influence of the applied pressure for two conversion rates (30%,40%) was studied for the three NF membranes tested. Mathematical models have been applied in order to understand the mechanism of transfer through the NF membranes and also to determine the structural parameters of these membranes. The membranes transport parameters (σ and P_s) during the transport of Na^+, Cl^- and Ca^{2+} ions were determined by applying SK model. The SHP model was tested to determine membrane effective pore size (r_p) and membrane thickness to porosity ($\Delta x/A^k$). A relative comparison of pore size was performed using Ca^{2+} which is a divalent cation which presents the highest stokes radius in comparaison to the Na^+ and Cl^- ions.

The fouling behavior of the three commercial NF membranes was also studied using Hermia fouling model and combined cake formation-complete pore blocking model in continuous mode.

The validation of the Hermia model and the combined model was achieved by analysing of the variance (ANOVA). The technical-economic study was performed for NF membranes on the basis of produced water with a sodium concentration of 150 mg/L.

Theory

Spiegler - Kedem model

In our study, the transport of Na^+, Cl^- and Ca^{2+} ions in NF membranes is described by SK model which is based on thermodynamics of irreversible systems. The equations obtained by SK which considers the membrane as a "black box" are:

$$J_v = Lp\left(\frac{dp}{dx} - \sigma\frac{d\pi}{dx}\right) \quad (1)$$

$$J_s = -\overline{P}\frac{dC_s}{dx} + (1-\sigma)C_s J_v \quad (2)$$

L_p : hydraulic permeability ;
P : pressure ;
x : distance ;
π : osmotic pressure ;
$\overline{P}$: local permeability of the solute ;
C_s : solute concentration in the membrane ;
σ : reflection coefficient .

According to (Eq.2), the flux of solute represent the sum of convective and diffusive terms. The concentration difference on the membrane and the permeate sides is responsible for the transport of solute by diffusion. The transport of solute by convection is due to the applied pressure gradient across the membrane.

By integrating of equations (Eq.1) and (Eq.2) and their combination with retention rate relation and for the limiting conditions (for x = 0, $C_m = C_f$, and for x = Δx, $C_m = C_p$) lead to the following equations:

$$Jv = Lp\,(\Delta P - \sigma\,\Delta\Pi) \quad (3)$$

$$R = 1 - \frac{C_p}{C_f} = \frac{\sigma(1-F)}{1-\sigma F} \quad (4)$$

with $F = \exp\left(\frac{(1-\sigma)J_v}{P_s}\right)$

F : dimensionless parameter ;
ΔP : transmembrane pressure in (bar) ;
ΔΠ : difference in osmotic pressure on either side of the membrane in (bar) ;
C_0 : concentration in feed in ($mg.L^{-1}$);
C_p : concentration in permeate in ($mg.L^{-1}$);
C_m : concentration in the membrane in ($mg.L^{-1}$) ;
L_p : hydraulic permeability of the membrane in ($L.h^{-1}.bar^{-1}$) ;
σ : reflection coefficient (dimensionless) ;
P_s : solute permeability in ($m.s^{-1}$).

When the structure and transport mechanism within the membrane is not fully understood, SK model can be used to describe the transport in the membrane. SK model is based on thermodynamics of irreversible systems [30]. In this model, electrostatic interactions between the membrane and the solute are generally considered negligible like when the solute is neutral or the membrane is uncharged.

NF membranes are mainly negatively or positively charged and are used by SK in several studies [31,32]. These studies showed that the concentration of the feed solution and the effective membrane charge are the parameters on which σ and P_s depend on.

Regardless the type of solute, charge, solvent and membrane, SK model can be used to predict the solute and solvent transport mechanism through the membrane.

Steric Hindrance Pore Model (SHP)

Steric Hindrance Pore (SHP) model was suggested by Nakao and Kimura, where pore model was expanded to understand more structural parameters [33]. The pore radius (rp) and thickness to porosity ratio ($\Delta x/A_k$) represent the structural parameters of membrane. Later, this model was modified successfully by Wang et al. for NF membranes [34]. Using SHP model, steric effect and frictional forces hinder the transport of spherical ions through cylindrical pores. The membrane parameters σ and P_s are determined using the following equations :

$$\sigma = 1 - SC\,(1 + (16/9)\,\alpha^2) \quad (5)$$
$$P_s = D * SD\,(A_k/\Delta x) \quad (6)$$

Where:

$$S_D = (1-\alpha)^2 \quad (7)$$
$$S_C = (1-\alpha)^2\,(2 - (1-\alpha)^2) \quad (8)$$
$$S_C = SD * (2 - (1-\alpha)^2) \quad (9)$$

α is the steric hindrance parameter given by (Eq.10) [35].

$$\alpha = r_s/r_p \quad (10)$$

r_s : Stokes cation radius ;
r_p : effective membrane pore radius.

With [24]:

S_D and S_C are respectively steric hindrance factor for diffusion and steric hindrance factor for convection.

S_D is defined by Oren and Biesheuvel as a partitioning coefficient at the membrane-solution interface [36].

D is the diffusivity.

Table 1. presents the Stokes radii of Cl^-, Na^+ and Ca^{2+} ions used in our calculations [37,38].

Table 1: Cl^-, Na^+ and Ca^{2+} Stokes radius [37,38].

Species	Cl^-	Na^+	Ca^{2+}
Stockes radius (nm)	0.121	0.184	0.310

In the pore model, Hagen-Poiseuille formula used for determining the pure water permeability Lp is given by:

$$Lp = \frac{r_p^2\left(\frac{A_k}{\Delta x}\right)}{8\mu} \quad (11)$$

μ represent the viscosity.

Hermia Model

Individual mechanisms of membrane fouling are specifically described by models suggested by Hermia [39]. For the frontal filtration models, Field et al. modified these models to calculate the dense shape and a scale (filtered) [40,41]. These authors added a deposit erosion parameter in order to allow for the shear from the recirculating permeate in tangential filtration [42]. The model presented by Hermia is one of the most common models in the literature for modeling membrane flux decline during constant pressure filtration and give also some information about membrane fouling mechanism [26].

At a constant pressure filtration, the flux decline can be expressed by the following equation [43,44] :

$d^2t/dV^2 = k(dt/dV)^n$ (12)

With:
V represent the volume of filtrate (permeate), t represent the time of operation, n and k represent constant kinetics parameters.
The equation of flux given by the expression:

$J = 1/A*dV/dt$ (13)

The expression of flux mentionned in (Eq. 13) is used to give the flux decline expression :

$dJ/dt = -k.J.(J.A)^{2-n}$ (Eq.14)
Table.2 gives for each value of n and k, the corresponding fouling mechanism :

Table 2: Four models of membrane fouling suggested by (Hermia,1982) [45,46]

Fouling mode	Cake formation n=0	Standard blockage n=3/2	Intermediate blockage n=1	Complete blockage n=2
Expression of permeate flux	$J_p = J_0/(2K_{cf}J_0^2t+1)^{1/2}$	$_Jp = 4_J0/(_{Ks}b_{J0}^{1/2}t+2)^2$	$J_p = J_0/(K_{ib}J_0 t+1)$	$J_p = J_0 \exp(-K_{cb} t)$
Equation	(15)	(16)	(17)	(18)

Combined Model : Cake Filtration-Complete pore Blocking

This model originates from the inability of a single fouling mechanism to explain the average behavior in permeate flux development. The model was first proposed by Ho and Zydney [27], and has since been simplified, modified or adjusted in various ways by different authors [45-47]. This model created using two rate of stages, as shown in the literature, there was an initial sharp drop in the first minutes due to pore blocking phenomena and then there was an accumulation of molecules on membrane surface forming a cake layer leading to a slower decrease in permeate flow. This model provides a continuous junction between the two types of fouling introduced by Hermia which are complete blocking and cake filtration. The most natural elucidation of membrane fouling deployed for combined model of a fouling prospect is revealed more efficient mechanism than those divided foulings which is composed by single one [45]. Each of these two models has a constant, Kcb represent the constant of the complete pore blocking model and Kcf represent the constant of the cake layer model.

The combined model equation is presented in Eq.19.

$$J = J_0 * \left(\frac{-K_{cb}}{K_{cf} J_0^2} \left(\left(1 + \left(2K_{cf} J_0^2 t\right)\right)^{0.5} - 1 \right) \right) / \left(1 + (25_{cf} J_0^2 t)\right)^{0.5} \quad (19)$$

In our study, the combined cake layer formation - complete blocking pore model is tested. The decrease in flux is due mostly by complete blocking when the value of K_{cf} is low. The decrease in flux is due mostly by cake filtration when the value of K_{cb} is low [28].

Statistical Analysis

In modeling process, the determining step is the validation of the Hermia and the combined models. A nalysis of the variance (ANOVA)is used to the validation of the Hermia and the combined models.

To present the evolution of the filtration process, the procedure consists to plot the graph of permeate flux versus time for the membranes tested. Therefore, according to the best correlation and the lowest error probability on the distribution function F below 5%, the values of Kcb,Ksb, Kib and Kcf of Hermia model and the values of Kcb and Kcf of combinded model are determined [48].

Experimental

Feed water Characteristics

Our study was conducted on M'rirt city water. The feed water characteritics are presented in Table.3.

Table 3: Feed water characteristics.

Parameter	Feed water	WHO Standards	Moroccan Standards
Temperature, °C	29	25	-
Turbidity, NTU	<3	<5	<5
pH	7.74	6.5-8.5	6.0-9.2
TDS, mg/L	1100	1000	1000-2000
Conductivity, µS/cm	2140	250	1300-2700
Alkalinity, mg/L	34.0	No constraint	200
Hardness, mg/L	125.65	200	500
Magnesium, mg/L	20.05	50	100
Calcium, mg/L	105.6	75	<500
Sulphate, mg/L	60.0	250	200
Chloride, mg/L	595	300	300-750
Sodium, mg/L	381	200	200

Unit Pilot Testing

The NF pilot plant (E 3039) used in our study is supplied by TIA Company (Technologies Industrielles Appliquées, France). All our study experiments were carried on continuous mode as mentioned in Figure 1. Manual valves were used to varying the applied pressure from 5 to 70 bars over the membrane.

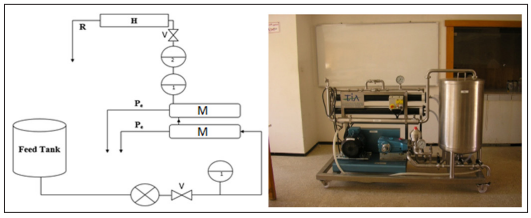

Figure 1: Picture and schematic diagram of the NF pilot plant (E 3039). V: pressure regulation valves, P: feed pump, T: tank, M: NF module, R: retentate recirculation, H: heat exchanger, Pe: permeate recirculation, 1: pressure sensor, 2: temperature sensor.

The parameters followed during our study are:
The permeation flux which is given by (Eq.20):

$$J_v = \frac{\Delta V}{S * \Delta t} \quad (20)$$

S: represent the surface of membrane (m^2);
ΔV (L) : represent the permeate volume receipt in Δt (s).
The Recovery rate Y (%) is expressed as:

$$Y(\%) = \frac{Qp}{Qf} * 100 \quad (21)$$

Q_p: represent the flow of permeate ($L.h^{-1}$);
Q_f: represent the flow of feed ($L.h^{-1}$).

The Salt retention is given by (Eq.22) :

$$R(\%) = \left(1 - \frac{Cp}{Cf}\right) * 100 \quad (22)$$

C_p : represent the concentration of solute in permeate (g/L) ;
C_f : represent the concentration of solute in feed water (g/L).

Characteristics of the Membranes

The pilot plant used in our study is equipped with two spiral wound modules and each module contains one membrane. The modules contains NF membranes of one type operating in series. The simple pass in continuous mode is the configuration tested. The pressure loss of each module is 1 bar. After each operation and according to the recommendations mentionned by the manufacturer, acidic and alkaline solutions were used for cleaning the membranes. Table.4 presents the characteristics of the membranes used in our study.

Table 4: Membranes Characteristics.

	NF270*4040	NF90*4040	TR60*4040
Material	Polyamide	Polyamide	Polyamide
Area (m^2)	7.6	7.6	6.8
Salt rejection (%)	> 97.0% [49]	97.0% [50]	-
Pmax (bar)	41	41	10
Cut-off (Da)	300 [51]	90	400

Analytical Methods

The temperature of M'rirt water city used in our study is 29°C. Standard methods were followed for determining analytically the permeate water parameters.

Results & Discussion

Applied Pressure Effect

Applied Pressure Effect on Permeate Flux

The configuration tested is simple pass in continuous mode and two recovery rates (30% and 40%) were tested to study the permeate flux variation in M'rirt water using three membranes. At these recovery rates, Figure 2 gives the permeate flux variation versus the applied pressure.

Figure 2 shows that the permeate flux augments practically linearly with the applied pressure following the Darcy's law. We can also see that the driving forces are improved with increasing the applied pressure and consequently surmount the membranes resistances [52]. Followed by TR60 and NF90 membranes, the NF270 membrane reveals a high permeate flux. This result may be attributed to the nature of membranes tested. The structures of NF270 and TR60 membranes are porous while that of NF90 membrane is denser and similar to that of RO membranes [52]. The sequence of the permeate flux is so: NF270 > TR60 > NF90.

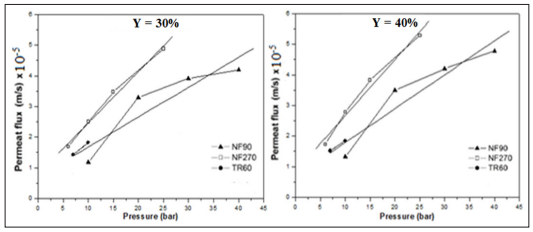

Figure 2: Permeate flux versus the applied pressure for the tested membranes for the recovery rates (Y = 30% and Y=40%).

The permeability of water for the NF membranes tested when M'rirt city water was used as the feed for the two conversion rates of 30% and 40% is given in Table.5.

Table 5: Permeability of the membranes tested for M'rirt city water

Conversion rate (%)	Membrane	M'rirt city water (m.s-1. bar-1) *10-6
30	TR60	6.8
	NF270*4040	7.96
	NF90*4040	5.2
40	TR60	5.2
	NF270*4040	8.42
	NF90*4040	7.15

The permeability L_p of the membranes tested don't vary during our study. Thus, during the experimental period, the membranes tested could be considered stable. As obtained for the permeate flux, the results of Table.4 show that NF270 membrane has a high permeabilty to M'rirt water for the two conversion rates of 30% and 40% followed by TR60 and NF90 membranes. This result can be attributed to the structure of the membranes tested. The structures of NF270 and TR60 are porous while that of NF90 membrane is denser and similar to that of RO membranes [52]. The sequense of the permeabilty of the tested membranes at two conversion rates (30% and 40%) is so: NF270 > TR60 > NF90. Also, the increase in the recovery rate lead to increase in the permeabilty of the membranes tested as shown in Table.4.

Pressure effect on permeate quality

In our work, the effect of pressure on sodium, chloride and calcium ions concentration in simple pass configuration in continuous mode was studied in two recovery rates (30% and 40%) for M'rirt city water. Figure 3 shows respectively for the membranes tested, the variation of the concentration of sodium, chloride and calcium ions in the permeate versus the applied pressure at two recovery rates (30% and 40%).

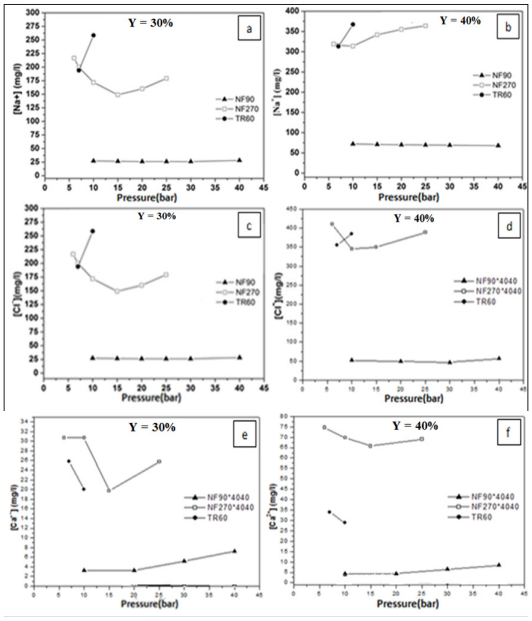

Figure 3: Variation of concentration of (a), (b) Na^+, (c), (d) Cl^- and (e), (f) Ca^{2+} with pressure for Y = 30% and Y=40% for the tested membranes.

The result obtained with NF90 membrane shows that the concentration of Na+ in the permeate is lower than that obtained with the two other NF membranes as shown in Figure 3a and 3b. The NF90 membrane has a structure close to that of the RO membranes [53].

Increasing recovery rate from 30% to 40% leads to an increase in the concentration of sodium for the tested NF membranes, which can be explained by the increase in the solvent flow [54]. The lowest concentration of sodium in permeate is obtained for NF90 membrane. As earlier seen, the structure of this membrane is close to those of RO membranes. For pres¬sure between 6 and 10 bars, the concentration of sodium obtained with NF270 membrane decreases and beyond the pressure of 10 bars, the concentration of Na+ increases. The result obtained can be attributed to the ion transport by diffusion which is predominant at low pressures. At high pressures, the ion transport is due to the convection mechanism transport [55].

For the membranes tested, the concentration of sodium and chloride ions obtained by the NF90 membrane is the lowest.

The concentration of sodium and chloride ions obtained by the NF270 membrane decreases at low pressures (lower pressure applied up to 10 bars) and increases beyond this pressure. The result obtained can be attributed to the ion transport by diffusion which is predominant at low pressures. At high pressures, the ion transport is due to the convection mechanism transport [56].

The concentration of sodium and chloride ions obtained by the TR60 membrane increases with the pressure for the two conversion rates of 30% and 40%. The concentration of sodium and chloride obtained, at a given pressure, increases with increasing conversion rate from 30% to 40%. The result obtained can be due to the increase in the permeate flow passing through the membrane.

For the conversion rate of 30%, the sodium concentration is 216.66 mg/L for the NF270 membrane at a pressure of 6 bars and 258.51 mg/L for the TR60 membrane at a pressure of 10 bars. These two values exceed the maximum admissible value (200 mg/L) fixed by the WHO, whereas for the other pressures applied, the sodium ion content is lower than the maximum admissible value fixed by the WHO.

For the two membranes NF270 and TR60 and for the conversion rate of 40%, the chloride ion content exceeds the maximum admissible value (250 mg/L) set by the WHO in the applied pressure range.

Figure 3e shows that for the conversion rate of 30%, the concentration of calcium in the permeate obtained by the membranes tested is much lower than the maximum admissible value (270 mg/L) of drinking water set by WHO in the applied pressure range and in particular for NF90 membrane. For the NF270 membrane, the calcium ion content in the permeate obtained is a little high in comparison with that obtained by the NF90 membrane and which reaches 30.70 mg/L at a conversion rate of 30% and at a pressure of 6 bars, and concerning the TR60

membrane, the calcium ion content reaches the value of 25.80 mg/L at a conversion rate of 30% and at a pressure of 7 bars.

For the two conversion rates of 30 and 40%, the calcium ion content in the permeate obtained by the three membranes tested is well below the maximum acceptable value (270 mg/L) for drinking water set by the WHO in the applied pressure range and in particular for the NF90 membrane. For the NF270 membrane, the calcium ion content in the permeate obtained is a little high in comparison with that obtained by the NF90 membrane and which reaches 30.70 mg/L and 74.70 mg/L at a conversion rate of 30 and 40% respectively at pressure of 6 bars, and for the TR60 membrane, the calcium ion content reaches the value of 25.80 mg/L and 34 mg/L at a conversion rate of 30 and 40% respectively at a pressure of 7 bars.

Models of Spiegler - Kedem and Steric Hindrance Pore Model of Spiegler - Kedem

To determine the optimal values of σ and Ps parameters which are analyzed by nonlinear regression using Origin Pro.8 (Figure 5,6) and for the tested membranes, the experimental data of sodium, chloride and calcium rejection versus the permeate volume flux were fitted applying SK model. For the membranes tested and for the two recovery rates (30% and 40%), the results of the rejection values show a good fit.

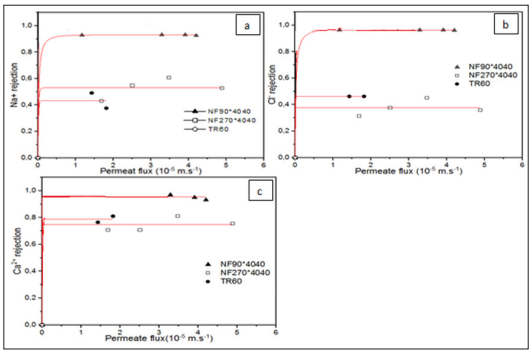

Figure 5: Permeate flux effect on rejection of (a) Na^+, (b) Cl^- and (c) Ca^{2+} for the tested membranes for conversion rate of 30%.

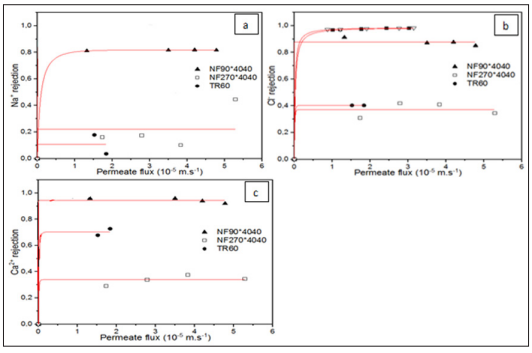

Figure 6: Permeate flux effect on rejection of (a) Na^+,(b) Cl^- and (c) Ca^{2+} for the tested membranes for conversion rate of 40%.

Table 4 gives for recovery rates (30% and 40%), the values of (σ, P_s) parameters determined for the three membranes tested.

In the case of Na^+, Cl^- and Ca^{2+}, and for recovery rates (30% and 40%), the NF90 membrane show a high value of σ which tends towards the unit. As previously mentioned, this membrane has a structure close to that of RO membranes.

In the case of the two recovery rates, lower σ values were obtained by TR60 and NF270 membranes. NF membranes have a low rejection of monovalent ions.

Table 6 shows also that the the recovery rate has an influence on the values of Ps and σ. The increase in recovery rate leads to a decrease in σ value for the three ions Na+, Cl- and Ca2+ and for the tested membranes.

Table 6: P_s and σ values obtained at recovery rates of 30% and 40% for the membranes tested

Membrane			TR60	NF270	NF90
Y=30%	Na^+	σ	0.43	0.59	0.93
		P_s ($m.s^{-1}$)	$5.33.10^{-8}$	$7.46.10^{-6}$	$1.97.10^{-7}$
	Cl^-	σ	0.46	0.41	0.96
		P_s ($m.s^{-1}$)	$2.20.10^{-7}$	$7.64.10^{-6}$	1.10^{-9}
	Ca^{2+}	σ	1	0.79	0.96
		P_s ($m.s^{-1}$)	$4.38.10^{-6}$	$3.49.10^{-6}$	$2.42.10^{-9}$
Y=40%	Na^+	σ	0.11	0.10	0.82
		P_s ($m.s^{-1}$)	$3.74.10^{-8}$	$2.21.10^{-8}$	$7.50.10^{-7}$
	Cl^-	σ	0.40	0.39	0.88
		P_s ($m.s^{-1}$)	$2.62.10^{-7}$	$6.66.10^{-6}$	1.10^{-9}
	Ca^{2+}	σ	1	0.37	0.94
		P_s ($m.s^{-1}$)	$7.17.10^{-6}$	$8.32.10^{-6}$	$3.16.10^{-9}$

Steric Hindrance Pore Model

For the three membranes tested, the pore radius rp based on Na^+, Cl^- and Ca^{2+} rejections data was determined from their σ values based on the SHP model using equations (5), (8) and (9). The value of rp was determined using the value of r_s stokes radius of Na^+, Cl^- and Ca^{2+} as shown in Table.1. The values of rp and Δx/Ak for Na^+, Cl^- and Ca^{2+} and for the two recovery rates (30% and 40%) using the NF membranes were determined from σ and P_s values based on the SHP model when water of M'rirt city was used as the feed and are presented in Table.7.

A comparison of pore size was performed with Ca^{2+} which is a divalent cation with the highest rs compared to the Na^+ and Cl^- ions tested for rp calculations, and also Ca^{2+} is attracted by the membrane with negative charge.

Table 7: Calculated α, r_p and $\Delta x/A_k$ for ions for the tested membranes.

Membrane			TR60	NF270	NF90
Y=30%	Na^+	α	0.54	0.65	1.10
		r_p (nm)	0.34	0.29	0.17
		$\Delta x/A_k$ (μm)	518	22.7	15.3
	Cl^-	α	0.56	0.53	0.91
		r_p (nm)	0.22	0.23	0.13
		$\Delta x/A_k$ (μm)	642	64.1	
	Ca^{2+}	α	1	1.17	0.91
		r_p (nm)	0.31	0.26	0.34
		$\Delta x/A_k$ (μm)	-	6.88	2550
	Na^+	α	0.26	0.25	0.79

		r_p (nm)	0.70	0.74	0.23
		$\Delta x/A_k$ (µm)	1610	2480	80.2
	Cl^-	α	0.52	0.52	0.84
		r_p (nm)	0.23	0.23	0.14
		$\Delta x/A_k$ (µm)	590	76.2	274
	Ca^{2+}	α	1.0	0.50	1.10
		r_p (nm)	0.31	0.62	0.28
		$\Delta x/A_k$ (µm)	-	23.7	2370

Table.7 shows that TR60 and NF270 membranes have a larger pore sizes and which can be considered as a loose NF membranes with an average pore size of repectively rp=0.29 nm and r_p=0.26 nm for conversion rate of 30%. For conversion rate of 40%, the average pore radius is rp=0.41 nm and r_p=0.53 nm respectively for TR60 and NF270 membranes. For NF270 membrane, this value is in the same range of the value obtained by the study realized by Zhu and al which is about of 0.42 nm. For TR60 membrane, these values of pore radius for the two conversions rates are greater than that obtained by Tahaikt and al which is about of 0.167 nm [57]. These membranes showed an average pore size relatively larger than the rs of Na^+ and Cl^- examined in this study for the two conversion rates (30% and 40%). This result show that rejection efficiency is least influenced by steric effect [53]. The average pore size of these membranes is relatively lower than Ca^{2+} stokes radius for the conversion rate of 30%, and relatively greater than rs of Ca^{2+} at the conversion rate of 40%.

Tables.5 and 6 show that the membranes TR60 and NF270 with larger pore sizes have lower values. On the other hand, membranes with higher P_s values have lower σ values Luo and Wan reported that NF270 membrane average pore radius rp is 0.43 nm [58]. It was found by Micari and al that the membrane NF270 has a pore radius of 0.507 nm [59]. In our study and at conversion rate of 40%, this membrane has an average pore size of 0.53 nm as found using the SHP model. Tahaikt et al reported that for NF270 membrane, the pore radius is about of 0.148 nm [53]. Also,as studied by Hilal et al the pore size of NF270 membrane was previously determined using atomic force microscopy [60]. These authors suggested that the pore size of NF270 membrane may be between 0.47-0.99 nm with a mean of 0.71 nm. In the conversion rate of 40%, the calculated pore size of NF270 membrane determined in our study was in concordance with other studies which confirms the validity of our calculations. Another structural parameter ($\Delta x/A_k$) determined in Table.6 was calculated using SHP model. The results of Table.6 shows that for TR60 membrane, the average value of $\Delta x/A_k$ is of about 580 µm and 1100 µm for conversion rate of 30% and 40% respectively. For NF270 membrane, the average of $\Delta x/A_k$ is of about 31.22 µm and 859.96 µm for conversion rate of 30% and 40% respectively. For NF membranes and according to the SHP model, r_p and $\Delta x/A_k$ structural parameters have a significant contribution to the membranes transport mechanism.

Table 6 shows that the average pore size of NF90 membrane is r_p=0.21nm at conversion rate of 30% and r_p=0.20nm at conversion rate of 40%.

For NF90 membrane, the average pore radius found by Zhu and al is of about 0.34 nm [57].

The pore radii of certain NF membranes as indicated in works showed that the pore radii of NF90 membrane was between 0.24-0.3 nm [61]. This value is slightly higher than that determined in our study.

Research realized by Ali Fatehizadeh et al reported that the average pore radius of NF90 membrane is of about 0.12 nm [23]. Studies realized by Tahaikt and al showed that the value of pore size of NF90 is of about 0.129 nm [53]. The value obtained in our study is greater than those obtained in these study.

Empirical measurement realized by Zeggar et al showed that the pore radii of NF90 membrane is of about 0.16 nm, which is slightly lower than the value obtained in our study [62].

Virgin membrane showed a significantly higher value of pore radius compared to that obtained in our study and these studies. The results obtained in our study can be explained by the kind of material deposited inside the membranes pores leading to the reduction of the pores radius [62].

We can note that the electric interaction between membrane charged surface and solute can explain the difference, except for NF270 membrane in the conversion rate of 40% in which the average pore raduis was in the same range as determined by several studies, between the calculated value found in the literature and that calculated in this study. In the SK and SHP models, the electric interaction phenomenon is neglected [53].

Indeed, the results of Table.6 shows that NF90 membrane have a value of average of ratio of $\Delta x/A_k$ is of about 955.76 µm for conversion rate of 30%, and 908.3 µm for conversion rate of 40%. Studies realized by Zeggar and al showed that the ratio of Δx/Ak is of about 2.55 µm [62]. Fatehizadeh and al investigated fluoride rejection by NF90 membrane obtained a value of 478 µm for the ratio of $\Delta x/A_k$ [23]. This factor may contributed to the relatively highest permeation of the NF tested membranes [37]. The SHP is not a good model for solutes or ions with reflection coefficient very close to unity or highly restricted permeation [24].

Hermia Model and Combined Model

The fouling phenomenon on the membrane process can be predicted using mathematical models. The fouling of membranes tested was studied by applying Hermia and combined cake filtration-complete pore blocking models. The purpose of our study is finding the fouling mechanism probably responsible for the reduction of water flux that occurs in the three NF membranes. The study was conducted in semi-batch configuration mode at conversion rate of 40% and pressure of 40 bar.

The four fouling mechanisms flux expressions of Hermia model modified by Field et al. (1995) with tangential filtration mode in membranes are presented in Table 2 [63]. In this model, we use the parameter flux versus time, and the initial value J0 of flux is set and then optimizing the values of K_{cf}, K_{sb}, K_{ib} and Kcb parameters. Hermia fouling models were fitted to the data found experimentally by using Origin Pro 8 software of each

filtration process with the purpose of determinig the best fouling model describing the fouling mechanism of membrane during nanofiltration of water of M'rirt city. The obtained results from the modeling of the fouling for the tested membranes are shown in Figure7a, b and c.

As shown in these figures, for the membranes tested, the permeate flux passes through three phases, in the first, the flux rate decreases rapidly due to the polarization of the concentration, then it decreases slightly, which corresponds to the beginning of the fouling and the last phase is characterized by a stable flux due to the complete fouling.

In our study and in corresponding to the work of Hermia and Tien et al. The pore blocking fouling mechanism is not rapid with NF270 membrane [64,65]. The pore blocking fouling mechanism is especially related to the porosity of the membrane and also to the stability of membrane's flux in comparison with other tested membranes.

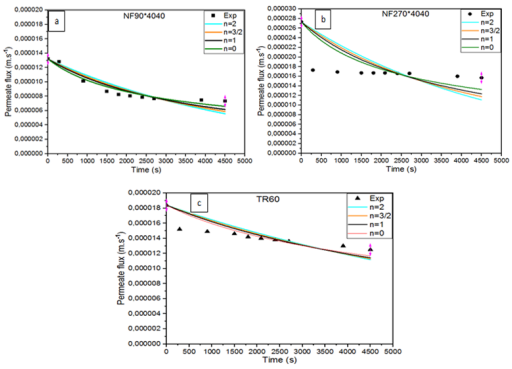

Figure 7: Experimental data and fouling mode for the tested membranes: (a) NF90, (b) NF270 and (c) TR60.

In our work, combined model, cake filtration and complete blocking pore mechanisms of Hermia model were fitted to the data found experimentally of M'rirt water city at constant pressure of 10 bar and in semi-batch configuration by using Origine Pro 8 software. The results of variation of experimental permeate flux data in company with predicted permeate flux data determined by modeling of the fouling using combined model, cake filtration and complete blocking pore mechanisms of Hermia model for the tested membranes are presented in the Figures.8a, b and c.

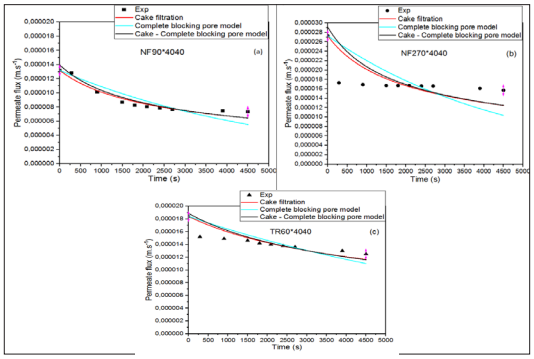

Figure 8: Experimental permeate flux data in company with predicted permeate flux data using combined fouling model, cake filtration and complete blocking pore mechanisms of Hermia model for the tested membranes. (a) NF90, (b) NF270 and (c) TR60.

The values of R-square (R^2), standard error and Ki for M'rirt water city at constant pressure corresponding to Hermia and combined models determined for the tested membranes are presented in Table.8. To evaluate the fitting degree of model and determining the type of pore blocking, the R-square values were used [66]. Highest value of R-square indicates that the model used is most appropriate for describing the fouling mechanism occured in the membranes[67].

Table 8: Values of R^2, standard error and K_i for M'rirt water city at constant pressure corresponding to Hermia and combined models for the tested membranes.

Model of Hermia									
	NF90*4040			NF270*4040			TR60*4040		
	K_i	R^2	Standard error	K_i	R^2	Standard error	K_i	R^2	Standard error
K_{cf}	$2.02.10^{6}$	0.94	$1.55.10^{5}$	$5.62.10^{5}$	0.15	$1.23.10^{5}$	$4.89.10^{5}$	0.62	$5.91.10^{4}$
K_{sb}	$6.20.10^{-2}$	0.85	$5.83.10^{-3}$	$4.6.10^{-2}$	No convergence	$9.14.10^{-3}$	$2.86.10^{-2}$	0.44	$3.42.10^{-3}$
K_{ib}	$1.98.10^{1}$	0.89	1.69	$1.06.10^{1}$	No convergence	2.18	$1.99.10^{1}$	0.51	$8.96.10^{-1}$
K_{cb}	$1.92.10^{-4}$	0.78	$1.85.10^{-5}$	$2.00.10^{-4}$	No convergence	$3.8.10^{-5}$	$1.11.10^{-4}$	0.37	$1.32.10^{-5}$
Combined model									
	NF90*4040			**NF270*4040**			**TR60*4040**		
K_{cf}	$2.09.10^{6}$	0.94	$3.01.10^{5}$	$2.31.10^{5}$	No convergence	$1.41.10^{-1}$	$3.01.10^{5}$	0.07	$1.34.10^{5}$
K_{cb}	$9.28.10^{-3}$		$3.41.10^{-2}$	0.0		$1.80.10^{5}$	0.0		$6.15.10^{-2}$

Results of Table.8 show that:

For the NF90 membrane, the cake layer formation mechanism (n = 0) shows the best values of R-square. The optimized parameter K_{cf} of a cake fouling mode reported in the literature for ultrafiltration process (UF) shows values lower than those obtained in our study.

The order of the optimized parameter K_{cf} is of 105, and the cake fouling mode is more predominant for greater value of K_{cf} [68]. The values of K_{sb}, K_{ib} and K_{cb} optimized parameters reported in the literature for UF process are significantly higher than those found in our study [68], which show that these types of fouling have a negligible contribution in our study. The obtained results can be explained by the nature of these membranes which have dense structure promoting surface fouling.

For TR60 and NF270 membranes, the R-squares (R^2) obtained by TR60 membrane are better than the R-squares obtained for NF270 membrane, which show that the model and the results found experimentally are in good fitting for the TR60 membrane than for the NF270 membrane.

For the tested membranes, the cake-formation mechanism (n = 0) describing well the experimental results and which can be due to the molecules accumulation on the membrane's surface [69]. The accumulation of molecules on membrane's surface leads to an increase in hydraulic resistance providing a decrease in permeate flux rate. The accumulation is important in the case of dense membranes and membranes with small pore sizes.

Figs.8a, b and c show the curves of experimental permeate flux data in company with predicted permeate flux data using combined fouling model, cake filtration and complete blocking pore mechanisms of Hermia model for the tested membranes. The symbols represent the experimental data whereas solid lines represent the combined model, cake filtration and complete pore blocking predictions.

At the starting of operation of filtration, the membranes tested showed a permeate flux reduction which may due to fast pore blocking of solutes on the membrane's surface and also to an increase in phenomenon of concentration polarization. During the operation of filtration, concentration polarization is important due to the accumulation of solutes on the surface of membrane. At later stages of filtration, The flux reduction is slow which can due to the formation of cake layer on the surface of membrane [69].

According to Table.8, combined model cake formation - complete blocking pore model has two unknown parameters which noted K_{cf} and K_{cb} that must be calculated by fitting the model to data found experimentally. The values of K_{cf} and K_{cb} calculated for the combined model for the membranes tested are presented in Table.8.

In the combined cake filtration-complete blocking model, the value obtained of the standard error was slightly lower than those obtained by the individuals cake formation and complete blocking pore models.

The values of the ratio $K_{cb}/K_{cf} * J_0 2$ obtained for the NF270 and TR60 membranes are respectively 0.0 and 0.37. This result indicate that the contributions of the cake filtration and complete blocking pore mechanisms are similar in the combined model. Earlier in the run, caking of solutes arriving at the membrane c an probably cause the fouling. Then complete blocking of smaller particles will succeed fouling mechanism which obstruct membrane pores. Therefore, complete blockage take place at the end of operation of filtration [70]. Whereas for NF90 membrane, this ratio is equal to 25.5 indicated that the contribution of the two mechanisms is not comparable in the combined model. As shown in Table.8, R-square value of the combined model with NF90 membrane is high and very near the unity. The K_{cf} value is high with comparison to K_{cb} value which can indicates that cake layer behaves more likely compared to complete blocking pore mechanism.

The results of the statistical analysis using ANOVA approach of the Hermia's and combined model for the membranes tested are showed in Table.9.

Table 9 : Statistical analysis of the Hermia and combined models for the membranes tested.

ANOVA STATISTICS								
Model of Hermia								
Global Assay	**K_i**	**DF**	**Sum of Squares**	**Mean Square**	**F Value**	**Prob > F**	**R-Square**	**Adj. R-Square**
NF90	K_{cb}	9	$9.33.10^{-12}$	$1.04.10^{-12}$	837.72	<0.0001	0.78	0.78
	K_{sb}	9	$6.53.10^{-12}$	$7.25.10^{-13}$	1201.73	<0.0001	0.85	0.85
	K_{ib}	9	$4.60.10^{-12}$	$5.11.10^{-13}$	1709.73	<0.0001	0.89	0.89
	K_{cf}	9	$2.53.10^{-12}$	$2.82.10^{-13}$	3109.34	<0.0001	0.94	0.94
NF270	K_{cb}	9	$1.60.10^{-10}$	$1.78.10^{-11}$	172.02	<0.0001	No convergence	No convergence
	K_{sb}	9	$1.38.10^{-10}$	$1.45.10^{-11}$	200.64	<0.0001	No convergence	No convergence
	K^{ib}	9	$1.19.10^{-10}$	$1.33.10^{-11}$	233.69	<0.0001	No convergence	No convergence
	K_{cf}	9	$8.97.10^{-11}$	$9.97.10^{-12}$	314.39	<0.0001	0.15	0.15
TR60	K_{cb}	9	$1.50.10^{-11}$	$1.76.10^{-12}$	1252.19	<0.0001	0.37	0.37
	K_{sb}	9	$1.32.10^{-11}$	$1.46.10^{-12}$	1428.39	<0.0001	0.44	0.44
	K_{ib}	9	$1.16.10^{-11}$	$1.29.10^{-12}$	1624.43	<0.0001	0.51	0.51
	K_{cf}	9	$9.06.10^{-12}$	1.10^{-12}	2080.89	<0.0001	0.62	0.62

Combined Model								
NF90	K_{cb}	8	$2.51.10^{-12}$	$3.14.10^{-13}$	1394.22	<0.0001	0.94	0.93
	K_{cf}							
NF270	K_{cb}	8	$2.22.10^{-10}$	$2.77.10^{-11}$	54.21	<0.0001	No convergence	No convergence
	K_{cf}							
TR60	K_{cb}	8	$2.21.10^{-11}$	$2.77.10^{-12}$	376.20	<0.0001	0.07	No convergence
	K_{cf}							

The evaluation of ANOVA analysis is carried out in consideration of the freedom degrees (DF), mean square, sum of squares , p-value and F-ratio. F-ratio is used for an indication of the variance of the data about the mean value [71]. F-ratio is used for qualitative evaluation, p-value is used for quantitative evaluation [72].

According to the results shown in Table.9, high R-square and adjusted R-Square values are obtained for NF90 membrane for Hermia and for the combined models. The values of R-square and those of Adj. R-Square are in good agreement which indicates high correlation between the experimental and predicted values. For this membrane, the value (0.94) of R-square and adjusted R-square is obtained for fouling by cake-formation characterized by the constant Kcf. For the combined model, the values of R-square and adjusted R-square obtained are respectively 0.94 and 0.93 which signifies that this model describes well the permeate flux experimental data versus time for NF90 membrane.

The values obtained by NF270 membrane for R-square and adjusted R-square are very low for Kcf corresponding to fouling by cake-formation as well as the non-convergence of R-square for the other constants of the Hermia model corresponding to standard blocking, intermediate blocking and complete pore blocking and also for the combined model. This indicates that these models do not describe the permeate flux experimental data versus time for this membrane. In our study and for NF270 membrane, these types of fouling have a negligible contribution in fouming of this membrane.

For the TR60 membrane, the value of 0.62 obtained for R-square and R-square adjusted for the constant Kcf of the Hermia model indicates that cake fouling is predominant. The low values of R-square and adjusted R-square indicate that the permeate flux experimental data versus time is not described by the combined cake-complete model.

These results are confirmed by the calculation of freedom degrees, p-value and the F-value.

When p-values are lower than 0.05, this indicate statistically significance of the models for the membranes tested.

When the F-value are far from the unity, the model or the models used provide a good explanation for the values obtained in the mean of the data [73].

The F-values obtained are (3109.34), (314.39) and (2080.89) for the NF90, NF270 and TR60 membranes respectively for fouling by cake-formation. The F-values are (1394.22), (54.21) and (376.20) for the NF90, NF270 and TR60 membranes respectively for the combined model.

Due to the good results shown by the NF90*4040 membrane, namely good retention of ions and particularly sodium ion and high flow of produced water, we will use this membrane in determining the cost of the produced cubic meter.

Economic Assessment

This section aims to determine the cost of the produced cubic meter. The calculation is carried out generally on the basis of the calculation of the cost of pre-treated water, the operating cost and the capital (investment) cost using NF90*4040 membrane. In this work, the cost of the produced cubic meter is based on the calculation of the cost of pre-treated water, the operating cost and the capital cost using NF90*4040 membrane. The produced cubic meter economic evaluation depends on factors like labor, site characteristics, raw water quality, type of technology, production capacity, membrane life, recovery rate, duration and factor of amortization [74,75].

The produced cubic meter economic assessment is achieved for a sodium removal plant with a daily capacity of 6480 m3 (corresponding to 270 m3 per hour). Following the moroccan standards in rural areas, water consumption is estimated for a popualtion of 80000 capita. According to a recovery rate of 83% and a concentration of 150 ppm of sodium in the produced water at a pressure pump of 10 bars, the plant design [76] was established using NF90*4040 membrane. In this study, the pre-treatment post is a conventional pre-treatment. In our study, we have adopted the same pre-treatment as that adopted in the drinking water treatment plant of M'rirt city followed by safety cartridge filtration with a speed filtration of 25.5 m/h and with a pore diameter of 5µm. Real data is used for the calaculation of the pre-treatment cost and is about of 0.3 €/m3 [76].

NF installation calculation of capital cost is achieved on the basis of experimentally value obtained for the flow rate.

In this study, the capital cost comprises the calculation of Heavy material cost, engineering cost, NF group cost, post-treatment cost, cost of auxiliary equipments and various services. We have adopted the ratios and the prices already decribed by El Azhar et al. [77].

The expressions adopted for determining of annual operating cost are those used by El Azhar et al [78]. The calculation of annual operating cost include cost of depreciation (or fixed costs), and maintenance operation cost, the interest cost of

invested capital, membrane replacement cost, chemical reagents cost, labor cost and the energy cost. In our study, The interest on invested capital was estimated at 3% per year. The annual membrane replacement rate was estmated at 5% of capital cost and for time operation of 6570 hours per year. The maintenance operation cost was estimated at 2% per year of the total capital cost. The chemical reagents cost was estimated at 0.5% of the total capital cost. The labor cost was estimated at 0.048 of the total capital cost. The depreciation period (lifetime of the plant) was fixed to 30 years. The average price of energy in Morocco is of 0.09 €/kWh and is used to calculate the energy cost.

In this work, a mixture of permeate with pre-treated water in the remineralization unit was used in order to obtain a sodium concentration of 150 mg/L in the produced water [76].

Table.10 presents a summary of NF plant data and costs using NF90*4040 membrane.

Table 10: NF plant data and costs.

Operating conditions	Nanofiltration
Pre-treatment (€/m^3)	0.3
Capital Cost (€)	
Heavy material	54000
Engineering	107400
NF group	408500
Post-treatment	1800
Auxiliary equipments	380726
Various services	10260
Total capital cost	962686
Operating cost (€/m^3)	
Depreciation of the installation	0.021
Interest on capital	0.018
Membranes replacement	0.010
Energy	0.036
Maintenance	0.013
Chemical reagents	0.003
Labor	0.030
Total operating cost	0.131
Total cost (€/m^3)	0.431

Table.10 show that the operating cost obtained by NF process using NF90*4040 membrane is 0.131 €/m^3. Tahaikt et al [79] estimated the operating cost at 0.1228 €/m^3 for a plant capacity of 2400 m^3 per day for the removal of fluoride ions from groundwater using NF process.

Amouamouha and Gholikandi [80] estimeted a cost per cubic meter produced water at 1.032 € using NF pilot plant of a capacity 60 m^3 per day for the nitrate removal from a naturally contaminated groundwater in Iran.

Costa et al. [81] estimated the cost of treated water at about 0.214 €/m^3 for NF plant with a daily capacity of 100000 m^3. Noureddine Elboughdiri et al [82] estimated at about 0.63 €/m^3 the cost of water produced by NF process with a daily capacity of 2000 m^3.

Conclusion

This work focused on the removal of three ions (Na^+, Cl^- and Ca^{2+}) drinking water of M'rirt city (Morocco) with comparing the rejection rate of three commercial NF membranes in continuous mode. For NF90 membrane, rejection exceed 80%. For the two conversion rates (30% and 40%) using NF270 and TR60 membranes, the rejection rate depends on the applied pressure. For the three membranes tested, SK equation fitting was used for each membrane in order to determine transport parameters. Experimental data and model predictions are in good agreement using SK model.

The calculated average pore size (rp) for the three NF membranes studied using SHP follows the classification order for conversion rate of 30% : r_p (TR60) > r_p (NF270) > r_p (NF90).

The calculated average pore size (rp) for the three NF membranes studied using SHP model follows the classification order for conversion rate of 40%: r_p (NF270) > r_p (TR60) > r_p (NF90).

The calculated average of ratio $\Delta x/A_k$ for the three NF membranes studied using SHP model follows the classification order for conversion rate of 30% :

$\Delta x/A_k$ (NF90) > $\Delta x/A_k$ (TR60) > $\Delta x/A_k$ (NF270).

The calculated of average of ratio of $\Delta x/A_k$ for the three NF membranes studied using SHP model follows the classification order for conversion rate of 30% :

$\Delta x/A_k$ (TR60) > $\Delta x/A_k$ (NF90) > $\Delta x/A_k$ (NF270).

The results of the Hermia model showed that the mechanism repondible of fouling occurred in the tested membranes is the cake formation model.

For NF90 membrane, the results showed that the combined cake formation-complete blocking pore model and experimental data are in good agreement which is confirmed by ANOVA statistical analysis.

In our work and using NF90*4040 membrane, the operating cost of the produced cubic meter is 0.131 €/m^3.

Acknowledgements

The authors express their thanks to ONEE Co. (Morocco) and TIA Co. (France) for their support.

References

1. Hachi T, Hachi M, Ech-Chafay H, Elghabassi M, Ettayea H, et al. Caractéristiques physicochimiques des eaux usées de la ville de M′rirt, (Maroc). Int. J. Innov. Appl. Stud. 2016. 791-803.
2. Silvio Borrelli, Michele Provenzano, Ida Gagliardi, Michael Ashour, Maria Elena Liberti, et al. Sodium Intake and Chronic Kidney Disease, International journal of Molecular Sciences. 2020.

3. Balaud A, Grimler C. Proposition d'une formation modulaire à destination des officinaux pour la prise en charge en ville des patients atteints de cancer-soins de support-cancer colorectal Doctoral dissertation, UHP-Université Henri Poincaré. 2010.
4. Mizéhoun-Adissoda, Carmelle. Apport alimentaire de sodium, potassium et iode, relation avec l'état nutritionnel au Bénin. Diss. Université de Limoges , Université d'Abomey-Calavi (Bénin) . 2015.
5. National Institutes of Health (NIH), Working group report on primary prevention of Hypertension, NIH Publication. 1993. 93-2669.
6. United States. Department of Agriculture. Human Nutrition Information Service. Dietary Guidelines Advisory Committee, United States. Dietary Guidelines Advisory Committee, United States. Office of Disease Prevention, Health Promotion. Nutrition and your health: dietary guidelines for Americans. US Department of Agriculture. 2000.
7. Pomrehn PR, Clarke WR, Sowers MF, Wallace RB, Lauer RM. Community differences in blood pressure levels and drinking water sodium. Am J. Epidemiol. 1983. 118: 60-71.
8. Faust HS. Effects of drinking water and total sodium intake on blood pressure, Am J Clin Nutrition. 1982. 35: 1459-1467.
9. Armstrong BK, Margetts BM, McCall MG, Binns CW, Campbell NA, Masarei JRL, Water sodium and blood pressure in rural school children. Arch Environ Health. 1982. 37: 236- 245.
10. Tuthill RW, Sonich C, Okun A, Greathouse D. The influence of naturally and artificially elevated levels of sodium in drinking water on blood pressure in school children. Journal Environ Pathol Toxicol. 1980. 3: 173-181.
11. Colditz GA, Willett WC. Epidemiological methods employed in the study of the influence of elevated drinking water sodium on blood pressure : a critique in : Proceedings of Conference on Inorganics in Drinking Water and Cardiovascular Disease. In : Calabrese et al. eds. Amherst, MA. 1985. 99.
12. Calabrese EJ, Tuthill RW. Elevated blood pressure and high sodium levels in the public drinking water, Arch Environ Health. 1977. 35: 200.
13. Calabrese EJ, Tuthill RW. The influence of elevated levels of sodium in drinking water on elementary and high school students in Massachusetts. Sci Total Environ. 1981. 18: 117-133.
14. Tuthill RW, Calabrese EJ. Elevated sodium levels in the public drinking water as a contributor to elevated blood pressure levels in the community. Arch Environ Health. 1979. 37: 197.
15. Fatula MI. The frequency of arterial hypertension among persons using water with an elevated sodium chloride content. 1967. 30: 134-136.
16. Dumont M. Annuaire des minéraux du Canada (AMC) : Sel, Ressources naturelles Canada, Secteur des minéraux et des métaux. 2008.
17. Wissem AYAD. Evaluation de la qualité physico-chimique et bactériologique des eaux souterraines : Cas des puits de la région d'El-Harrouch (WILAYA DE SKIKDA), Thèse de Doctorat, Université Badji Mokhtar – Annaba, Algérie. 2017.
18. Đuković J, Đukić B, Lazić D & Marsenić M. Tehnologija vode, Zvornik: Univerzitet u Istočnom Sarajevu, Tehnološki fakultet. 2000.
19. Wu D, Hu Y, Liu Y & Zhang R. Review of Chloride Ion Detection Technology in Water, Applied Sciences. 2021. 11: 11137.
20. Guidelines for Drinking-water Quality 4th Edition, Geneva, Switzerland,World Health Organization. 2017.
21. Othman NH, Alias NH, Fuzil NS, Marpani F, Shahruddin MZ, et al. A Review on the Use of Membrane Technology Systems in Developing Countries, Membranes. 2022. 12: 30.
22. Tian J, Zhao X, Gao S, Wang X, Zhang R. Progress in Research and Application of Nanofiltration (NF) Technology for Brackish Water Treatment, Membranes. 2021. 662.
23. Fatehizadeh A, Amin MM, Sillanpää M, Hatami N, Taheri E, et al. Modeling of fluoride rejection from aqueous solution by nanofiltration process: single and binary solution. Desalination and Water Treatment. 2020. 193: 224-234.
24. Nair RR, Protasova E, Strand S, Bilstad T. Implementation of Spiegler-Kedem and Steric Hindrance Pore Models for Analyzing Nanofiltration Membrane Performance for Smart Water Production, Membranes. 2018. 8: 78.
25. Matin A, Laoui T, Falath W, Farooque M. Fouling control in reverse osmosis for water desalination & reuse: Current practices & emerging environment-friendly technologies. Science of the total Environment. 2021. 765: 142721.
26. Janina Piekutin. The Identification of Fouling in Reverse Osmosis in the Treatment of Water with Petroleum Substances, Water. 2021. 1092.
27. Ho CC, Zydney AL. A combined pore blockage and cake filtration model for protein fouling during microfiltration. Journal of Colloid and Interface Science. 2000. 232: 389-399.
28. Bolton G, LaCasse D, Kuriyel R. Combined models of membrane fouling: Development and application to microfiltration and ultrafiltration of biological fluids. Journal of Membrane Science. 2006. 277: 75-84.
29. Kazemimoghadam M, Amiri-Rigi Z. Application of combined cake filtration-complete blocking model to ultrafiltration of skim milk. Journal of Water and Environmental Nanotechnology. 2017. 2: 311-324.
30. Jye LW, Ismail AF. Nanofiltration Membranes-Synthesis, Characterization and Applications , CRC Press, Taylor & Francis Group : Boca Raton, FL, USA. 2017.
31. Gilron J, Gara N, Kedem O. Experimental analysis of negative salt rejection in nanofiltration membranes, J. Membr. Sci. 2001. 185: 223-236.
32. Diwara CK, Lo S, Rumeau M, Pontie M, Sarr O. A phenomenological mass transfer approach in nanofiltration of halide ions for a selective defluorination of brackish drinking water, J. Membr. Sci. 2003. 219: 103-112.
33. Edwin Wallace. The use of nanofiltration for separation of heavy metals from wastewater, Doctoral Dissertation, University of Pardubice. 2020.
34. Wang XL, Tsuru T, Togoh M, Nakao SI, Kimura S. Evaluation of pore structure and electrical properties of nanofiltration membranes, J. Chem. Eng. Jpn. 1994. 28: 186-192.
35. Kukučka M, Kukučka Stojanović N. Intrinsic Dependence of Groundwater Cation Hydraulic and Concentration Features on Negatively Charged Thin Composite Nanofiltration Membrane Rejection and Permeation Behavior, Membranes. 2022. 12: 79.

36. Oren YS, Biesheuvel PM. Theory of ion and water transport in reverse-osmosis membranes. Physical Review Applied. 2018. 9: 024034.
37. Rozali S, Safari NH, Hassan AR, Ahmad M, Yunus RM. Assessment on Performance-properties of Asymmetric Nanofiltration Membranes from Polyethersulfone/n-Methyl-2-pyrrolidone/water Blends with Poly (vinyl pyrrolidone) as Additive. Periodica Polytechnica Chemical Engineering. 2022. 66: 54-69.
38. Hussain A, Nataraj S, Abashar M, Al-Mutaz I, Aminabhavi T. Prediction of physical properties of nanofiltrationmembranes using experiment and theoreticalmodels, J.Membr. Sci. 2008. 310: 321-336.
39. Khan IA, Lee YS, Kim JO. A comparison of variations in blocking mechanisms of membrane-fouling models for estimating flux during water treatment, Chemosphere. 2020. 259.
40. Hermia J. Constant pressure blocking filtration laws-application to power-law non-Newtonian fluids, Trans. Inst. Chem. Eng. V. 1982. 60: 183-187.
41. Field RW, Wu D, Howell JA, Gupta BB. Critical flux concept for microfiltration fouling, J. Membr. Sci. 1995. 100: 259-272.
42. Jarusutthirak C, Mattaraj S, Jiraratananon R. Influence of inorganic scalants and natural organic matter on nanofiltration membrane fouling, J. Membr. Sci. 2007. 287: 138-145.
43. Farhad Mansourizadeh, Reza Yegani, Ali Akbari. Analysis of Hermia fouling models for membrane prepared from blending of HDPE and poly (ethylene glycol) for humic acid filtration, The 12th International conference on Membrane Science and Technology. 2015.
44. Aryanti N, Nafiunisa A, Kusworo TD, Wardhani DH. Micellar-enhanced ultrafiltration using a plant-derived surfactant for dye separation in wastewater treatment. Membranes. 2020. 10: 220.
45. de la Casa EJ, Guadix A, Ibáñez R, Camacho F, Guadix EM. A combined fouling model to describe the influence of the electrostatic environment on the cross-flow microfiltration of BSA. Journal of membrane science. 2008. 318: 247-254.
46. Taniguchi M, Kilduff JE, Belfort G. Modes of natural organic matter fouling during ultrafiltration. Environmental science & technology. 2003. 37: 1676-1683.
47. Yuan W, Kocic A, Zydney AL. Analysis of humic acid fouling during microfiltration using a pore blockage–cake filtration model. Journal of Membrane Science. 2002. 198: 51-62.
48. Bassirou MH, Benkortbi O, Hamadache M, Hanini S, Amrane A. New approach of the fouling process modeling in tangential filtration on cake, Desalination and Water Treatment. 2017. 74: 71-86.
49. Tahaikt M, Elazhar F, Mohamed I, Zeggar H, Taky M, et al. Comparison of the performance of three nanofiltration membranes for the reduction of fluoride ions: application of the Spiegler–Kedem and Steric Hindrance Pore Models. Desalination and Water Treatment. 2021. 240: 14-23.
50. Fishman MJ, Downs SC. Methods for analysis of selected metals in water by atomic absorption. US Government Printing Office. 1966.
51. Centre d'expertise en analyse environnementale du québec, Détermination de la turbidité dans l'eau: méthode néphélémétrique. MA.103-Tur. 1.0, Rév. 4, Ministère du Développement durable, de l'Environnement et des Parcs du Québec. 2009. 10.
52. Asif Husain, Theoretical Basis of Analysis: Complexometric Titrations, Department of Pharmaceutical Chemistry,Faculty of Pharmacy. 2007.
53. Lhassani A. Rumeau M, Benjelloun D and Pontié M. Selective demineralization of water by nanofiltration, Application to the defluorination of brackish water, Water Research. 2001. 35: 3260-3264.
54. Zhu H, Hu B, Yang F. Removal of Sulfadiazine by Polyamide Nanofiltration Membranes: Measurement, Modeling and Mechanisms, Membranes. 2021. 11: 104.
55. Luo J, Wan Y. Effect of highly concentrated salt on retention of organic solutes by nanofiltration polymeric membranes, J. Membr. Sci. 2011. 372: 145-153.
56. Micari M, Diamantidou D, Heijman B, Moser M, Haidari A, et al. Experimental and theoretical characterization of commercial nanofiltration membranes for the treatment ofion exchange spent regenerant, Journal of Membrane Science. 2020. 606.
57. Hilal N, Al-Zoubi H, Darwish N, Mohammad A. Characterisation of nanofiltration membranes using atomic force microscopy, Desalination. 2005. 177: 187-199.
58. Yagnaseni Roy. The influence of temperature on ion transport in nanofiltration membranes, Massachusetts institute of technology, Thesis. 2018.
59. Zeggar H, Touir J, El-Ghzizel S, Elazhar F, Tahaikt M, et al. Characterization of ion transfer and modeling of fouling in nanofiltration and reverse osmosis membranes. Desalination and Water Treatment. 2021. 240: 2-13.
60. Charfi A, Ben Amar N, Harmand J, Analysis of fouling mechanisms in anaerobic bioreactors, Water Research. 2012. 2637-2650.
61. Hermia J. Constant pressure blocking filtration laws -application to power-law non-Newtonian fluids. Institute of Chemical Engineering. 1982. 60: 183-187.
62. Tien C, Ramarao BV, Yasarla R. A blocking model of membrane filtration. Chemical Engineering Science. 2014. 111: 421-431.
63. Zhang W, Ding L. Investigation of membrane fouling mechanisms using blocking models in the case of shear-enhanced ultrafiltration, Sep. Purif. Technol. 2015. 141: 160-169.
64. Cancinomadariaga B, Ruby R, Castro CA, Torrico JS, Riquelme ML. Analysis of the membrane fouling mechanisms involved in clarified grape juice ultrafiltration using statistical tools. Ind. Eng. Chem. Res. 2012. 51: 4017-4024.
65. Amine Charfi, Étude d'un procédé membranaire de traitement des eaux usées: effet des paramètres biotiques et abiotiques sur le colmatage de la membrane, Sciences de l'ingénieur [physics], Université de Carthage. 2014.
66. Biswajit Sarkar. A combined complete pore blocking and cake filtration model during ultrafiltration of polysaccharide in a batch cell, Journal of Food Engineering. 2013. 116: 333-343.
67. Kazemimoghadam M, Amiri-Rigi Z. Application of combined cake filtration-complete blocking model to ultrafiltration of skim milk. Journal of Water and Environmental Nanotechnology. 2017. 2: 311-324.

68. Corbatón-Báguena MJ, Vincent-Vela MC, Gozálvez-Zafrilla JM, Álvarez-Blanco S, Lora-García J, et al. Comparison between artificial neural networks and Hermia's models to assess ultrafiltration performance. Separation and Purification Technology. 2016. 170: 434-444.
69. Kaya Y, Dayanir S. Application of nanofiltration and reverse osmosis for treatment and reuse of laundry wastewater. Journal of Environmental Health Science and Engineering. 2020. 18: 699-709.
70. Myers RH, Montgomery DC, Anderson-Cook CM, Response Surface Methodology: Process and Product Optimization Using Designed Experiments, third ed., John Wiley & Sons Inc., Hoboken, New Jersey. 2009.
71. Tamim Y, The economic for desalination, contemporary water research and education. 2005. 39-45.
72. El- Dessouky H, Ettoumy H. Study on water desalination technologies, prepared for ESCW. 2001.
73. Noureddine ZOUHRI, Fatima Zahra ADDAR, Mustapha TAHAIKT, Mahacine ELAMRANI, Azzedine ElMIDAOUI et al. Techno-economic Study and Optimization of The Performance of Nanofiltration and Reverse Osmosis Membranes In Reducing The Salinity of M'rirt Water City (MOROCCO), Desalination and Water Treatment. 2024.
74. Elazhar F, Tahaikt M, Achatei A, Elmidaoui F, Taky M, et al. Economical evaluation of the fluoride removal by nanofiltration. Desalination. 2009. 249: 154-157.
75. Elazhar F, Touir J, Elazhar M, Belhamidi S, El Harrak N, et al. Techno-economic comparison of reverse osmosis and nanofiltration in desalination of a Moroccan brackish groundwater, Desalination and Water Treatment. 2014. 1-7.
76. Tahaikt M, El-Ghzizel S, Essafi N, Hafsi M, Taky M, et al. Technical-economic comparison of nanofiltration and reverse osmosis in the reduction of fluoride ions from groundwater: Experimental, modeling, and cost estimate. Desalination and Water Treatment. 2021. 216: 83-95.
77. Amouamouha M, Badalians Gholikandi G. Performance investigation and cost evaluation of nanofiltration membranes in groundwater remediation, Proceedings of the 5th International Conference. 2018.
78. Costa AR, de Pinho MN, Performance and cost estimation of nanofiltration for surface water treatment in drinking water production, Desalination. 2006. 55-65.
79. Noureddine Elboughdiri, Renzun Cosma, Abdelfattah Amari, Velibor Spalevic, Branislav Dudic, et al. Evaluating the feasibility of direct contact membrane distillation and nanofiltration in ground water treatment through a techno economic analysis, Applied Water Science. 2024.
80. Al-Qadami EHH, Ahsan A, Mustaffa Z, Abdurrasheed AS, Yusof KW, et al. Nanofiltration membrane technology and its applications in surface water treatment: A review, Journal of Desalination and Water Purification. 2020.
81. Garba Y, Taha S, Gondrexon N, Dorange G. Recueil de conférences du 7éme colloque AQUATEC, Limoges. 1996.
82. Mänttäri M, Pekuri T, Nystrom M. NF270 a new membrane having promising characteristics and being suitable for treatment of dilute effluents from the paper industry, Journal of Membrane Science. 2004. 242: 107-116.